Simulation studies of fault ride through capability of converter connected wind turbines in unsymmetrical faults

Anssi Mäkinen, SGEM deliverable 5.1.18

1. Introduction

In this report, the operation full-power converter connected of wind turbine under asymmetrical faults is studied. The aim is to investigate how different synchronizing methods and wind turbine control methods impact on the fault current response of the wind turbine. The comparison is done between three different synchronizing methods which are synchronous reference frame – phase locked loop (SRF-PLL), decoupled double synchronous reference frame – phase locked loop (DDSRF-PLL) and dual second order generalized integrator – frequency locked loop (DSOGI-FLL). In addition, three different control methods under asymmetrical voltage dip are studied which are active power prioritization, reactive power prioritization and combination of those two. Detailed discussion about the synchronizing methods can be found from the reference [1].

Wind turbine system using network side converter in network voltage reference frame

The wind turbine system model including the control system of the network side converter (NSC) oriented to the network voltage reference frame is shown in Fig. 1. The target of this study is to analyse the synchronization of the wind turbine system. It is not necessary to model the mechanical parts of the wind turbine in detail because the mechanical time constants are much greater than time constants related to synchronization. Thus, the wind turbine mechanical parts, generator and the generator side converter (GSC) are modelled as a current source i_{WT} in the DC-link of the frequency converter where the generated electrical power p_{gen} is controllable. This assumption is valid because the GSC is able to control output power of the generator. The value for i_{WT} is calculated from: [1]

$$i_{WT} = \frac{p_{gen}}{u_{dc}} \tag{1}$$

where u_{dc} is the DC-link voltage. The braking chopper is modelled in the DC-link of the frequency converter. The switch activating the chopper is closed when the DC-link voltage increases above 1250V and the surplus energy is dissipated in the resistance R_{dc}. Thus the converter protects itself from overvoltage which would destroy the DC-link capacitor C_{dc}.

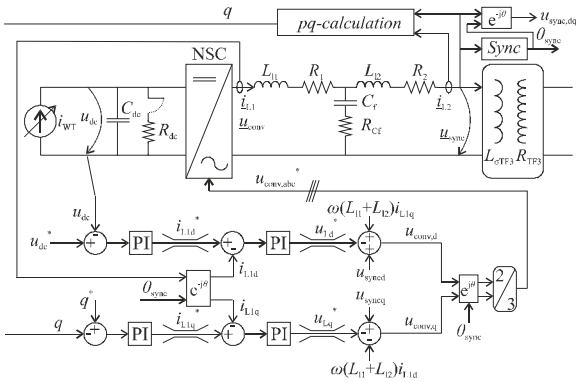

Fig. 1. Wind turbine system model and control system of the NSC.

The vector control of NSC is done in the reference frame synchronized to the connection point voltage $\underline{u}_{sync}$. The phase angle of the fundamental frequency component of the voltage is the output of the block *Sync*. The internal angular frequency is limited to 2*π*50±10Hz in all synchronization systems in this study. The aim of the dc-link voltage controller is to keep constant dc-link voltage, thereby ensuring that the generated active power p_{gen} is fed into the network. The output of the dc-link voltage controller is the d-component of the converter current $i_{L1,d}$. Reactive power controller gives the reference of q-axis component of the grid side current $i_{L1,q}^*$ as an output. The calculation of instantaneous reactive power q is performed in the *pq-calculation* block. The reference currents i_{L1d}^* and i_{L1q}^* are compared to the measured value and the error fed to the current controllers. The outputs of the current controllers are the voltage components over LCL-filter inductors u_{Ld} and u_{Lq}. Removing the cross-coupling terms and with the help of the measured connection point voltage components u_{syncd} and u_{syncq}, the NSC voltage reference components u_{NSCd}^* and u_{NSCq}^* can be presented.

The switching action of the NSC is not taken into account in this study and the NSC is assumed to produce the reference voltage $\underline{u}_{NSC}$ ideally. However, the design of the LCL-filter was based on the switching frequency f_{sw} of 3.6 kHz. The resonance frequency of the filter f_{res} is 1072 Hz when the transformer inductance $L_{\sigma TF3}$ is taken into account. The used parameter values for the LCL-filter are shown in Table 1. The parameters of the NSC are depicted in Table 2 and the controller parameters are expressed in Table 3. The d- and q-axis current controllers use same parameters. It should be noted that limit values are vector limit values i.e. peak value of the phase quantity.

Table 1. LCL filter parameters.

L_{l1}=300µH	L_{l2}=83µH	R_1=2.4mΩ	R_2=1mΩ	C_f=0.2mΩ	R_{Cf}=0.25Ω

Table 2. NSC parameters.

u_{dc}^*=1100V	C_{dc}=22mF	R_{dc}=0.2Ω

Table 3. PI control parameters.

	Current controller d/q		**DC-link controller**	**Reactive power controller**
Gain	k_i=0.57	k_i = 0.51	k_{udc} = 4.5	k_q = -0.45
Integration	T_{i_i}=1.5ms	T_{i_i} = 7ms	T_{i_udc} = 50ms	T_{i_q} = 40ms
Sampling time	T_{s_i} = 100µs	T_{s_i} = 100µs	T_{s_udc} = 100 µs	T_{s_q} = 100 µs

Upper limit	$\lvert \underline{u}_{Lmax} \rvert$ = 100V	$\lvert \underline{u}_{Lmin} \rvert$ = -100V	$\lvert \underline{i}_{L1dmax} \rvert$ = 670 A	$\lvert \underline{i}_{L1qmax} \rvert$ = 600 A
Lower limit			$\lvert \underline{i}_{L1dmin} \rvert$ = -670 A	$\lvert \underline{i}_{L1qmin} \rvert$ = -600 A

Network model

The network model used in the study is shown in Fig. 2. The 110 kV transmission network consists of two parallel feeders. The feeder 1 represents weak feeder having much greater impedance compared to feeder 2. The feeder 1 impedance values including transformer TF1 are chosen so that when circuit breakers Cb_{f21} and Cb_{f22} are opened the feeder impedance equals to the impedance found in real Finnish network. The feeder 2 impedances have been similarly measured from the real Finnish grid. [1]

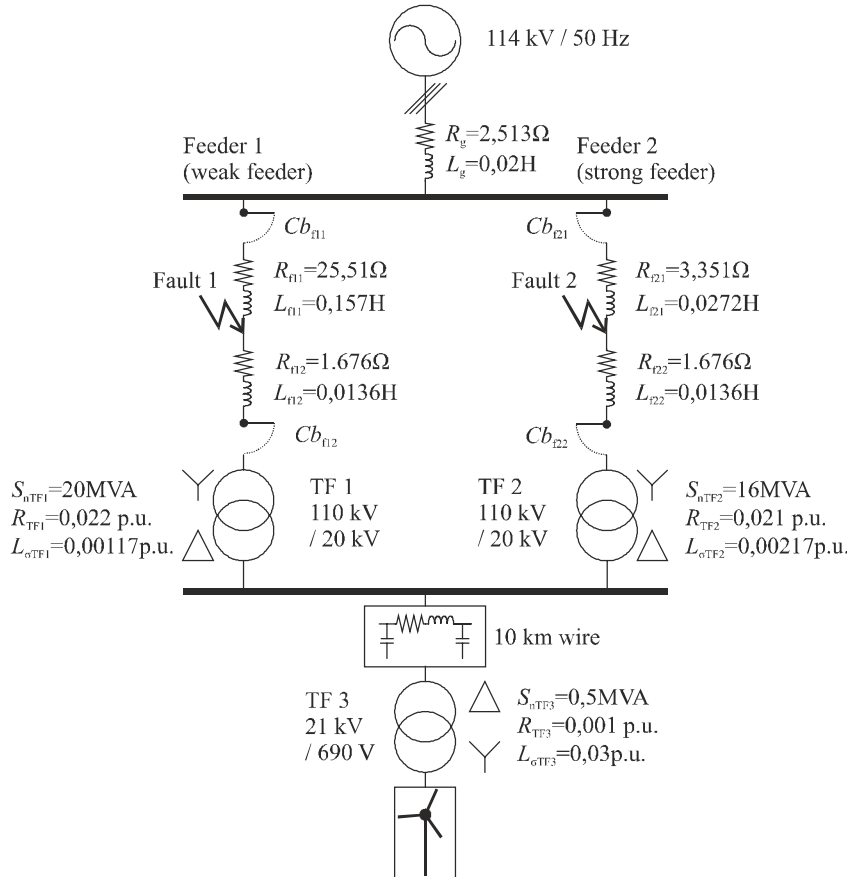

Fig. 2. Network model with used parameters.

Simulation results

It is assumed that during voltage dip the network protection is based on distance protection with the following operation procedure. The a-phase-to-ground fault occurs in point Fault 2 at 0.3s. After 200 ms from the beginning of the fault the circuit breaker Cb_{f22} opens and the WT currents flow through weak feeder 1 and through circuit breaker Cb_{f21}. After 300ms from the fault beginning at time 0.6s the Cb_{f21} opens and the fault is cleared from the WT viewpoint. Three different control principles of WT during the fault is used. In first, the active power is prioritized and the converter current reference i_q^* is set to zero. In the second case, the reactive power is prioritized and the reference of NSC current q-component is increased to constant 591A

(418A RMS) and the current i_{WT} in Fig. 14 is set to zero. In the third case, the WT is assumed to operate at full power during the fault and the reference for reactive power q^* is set to zero. [1]

The fundamental frequency negative sequence component and harmonic components from 2nd to 20th of the converter currents are measured and integrated (summed) in order to measure the quality of the generated current. In other words, the converter current is more close to pure sine wave throughout the fault when the harmonic integral is small. The harmonic integrals are normalized using normal (Gaussian) distribution and from now on the term harmonic integral corresponds to normalized harmonic integral. In addition, the error measures of d- and q-axis current controllers are integrated and normalized using normal distribution.

Nominal wind turbine operation with zero i_q^*

The d- and q- axis current controller error integrals and harmonic integrals using three different synchronizing methods are shown in Fig. 3a, 3b and 3c. The best performance regarding to the current controller errors and converter current harmonics is achieved using DSOGI-FLL with SOGI gain k=0.5. The worst performance appears using SRF-PLL. The connection point voltages, converter currents and zoomed converter currents when SRF-PLL is used are shown in Figs. 4a, 4b and 4c, respectively. Same measures when DSOGI-FLL is used are shown in Figs. 4d, 4e and 4f.

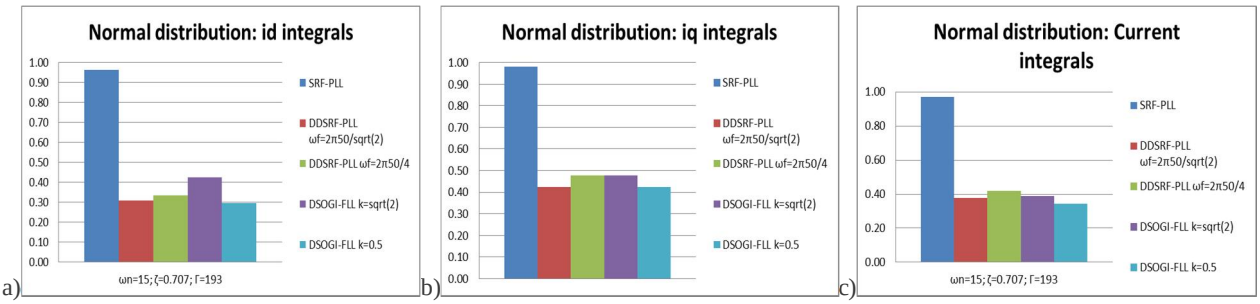

Fig. 3. a) d-axis current controller error integrals, b) q-axis current controller error integrals, c) harmonic integrals during phase to ground fault.

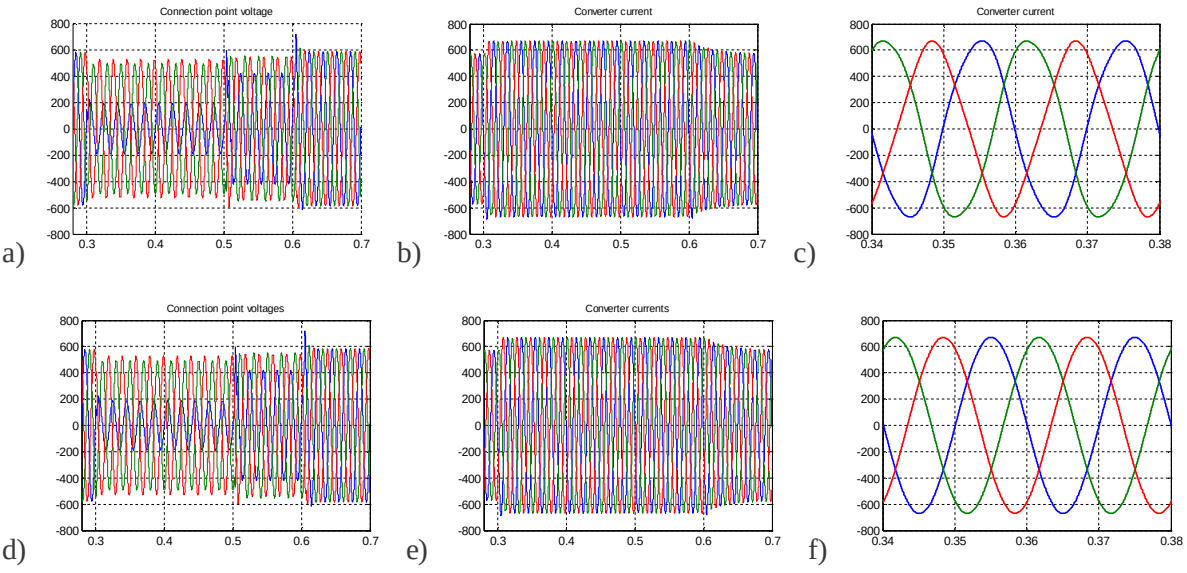

Fig. 4. SRF-PLL: a) connection point voltages, b) converter currents, c) zoomed converter currents; DSOGI-FLL: d) connection point voltages, e) converter currents, f) zoomed converter currents.

It can be seen that the WT can ride through the fault using both synchronization methods. The main difference can be noticed from Figs. 4c and 4f. When SRF-PLL is used the negative sequence component of the connection point voltage interfere the grid synchronization angle causing additional harmonic components to the converter currents. When DSOGI-FLL is used the SOGI filters out the impact of negative sequence component more efficiently. Thus, the converter currents are more sinusoidal.

The converter current d-axis component and its reference are shown in Figs. 5a and 5c when SRF-PLL and DSOGI-FLL is used, respectively. The q-axis components are shown in Figs. 5b and 5d. The difference between Figs. 5a and 5c are of no importance. However, the 100 Hz component caused by the negative sequence component of the grid voltage is clearly visible in Fig. 5b. The impact of the negative sequence component is filtered to a large extend when DSOGI-FLL is used as shown in Fig. 5d.

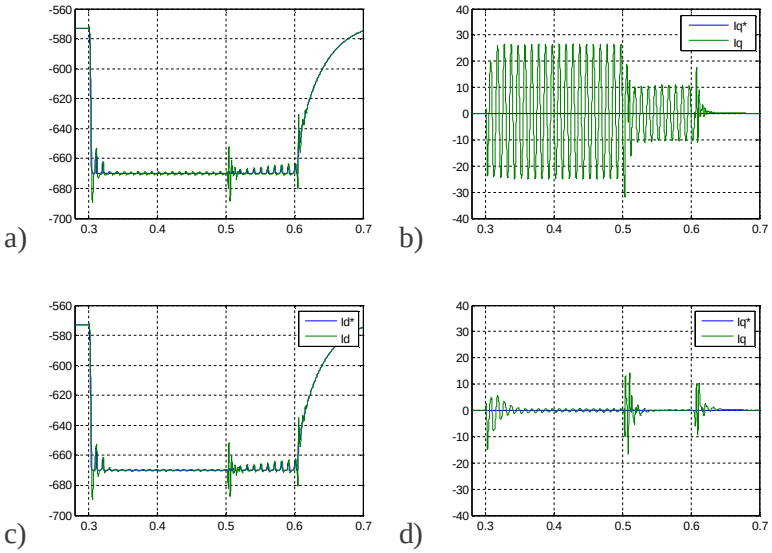

Fig. 5. SRF-PLL: a) d-axis converter current and its reference, b) q-axis converter current and its reference; DSOGI-FLL: c) d-axis converter current and its reference, d) q-axis converter current and its reference.

The frequency of the SRF-PLL during the grid fault is shown in Fig. 6a. Also here, the negative sequence component causes the 100 Hz oscillations. The angle of the SRF-PLL is achieved after integration of this angular frequency. Thus, even though the current d- and q-component references are constants the converter current contains additional harmonics. The Fig. 4c shows that the angular frequency is nearly constant when DSOGI-FLL is used. The DC-link voltage and its reference values are shown in Figs. 6b and 6d when SRF-PLL and DSOGI-FLL is used, respectively. The difference between the results in 6b and 6d are of no importance. It can be noticed that after the fault the DC-link voltage increase and the DC-link chopper is activated. The reason for DC-link increase in DC-link voltage is the decrease in positive sequence component of the network voltage. Thus, the NSC cannot feed the power generated by the wind turbine to the network due to the current limits of the NSC.

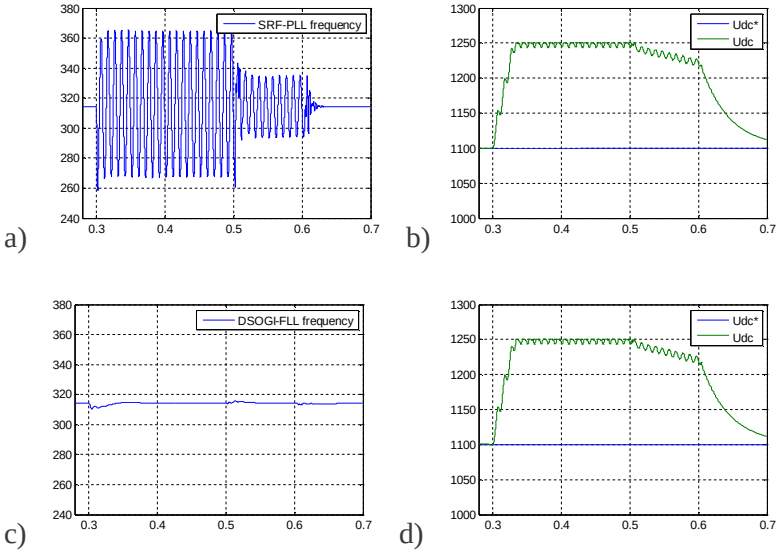

Fig. 6. SRF-PLL: a) angular frequency, b) DC-link voltage reference and measured value; DSOGI-FLL: c) angular frequency, d) DC-link voltage reference and measured value.

Nominal reactive current with zero i_{WT}

The d- and q- axis current controller error integrals and harmonic integrals are shown in Fig. 7a, 7b and 7c. The best performance regarding to the current controller errors is achieved using DSOGI-FLL with SOGI gain k=sqrt(2). The worst performance appears using SRF-PLL. The best performance for current integrals is achieved using SRF-PLL and the worst performance appears using DDSRF-PLL with ωf=2π50/4. However, the results in Fig. 7c are somewhat misleading due to the fact that the values of harmonic integrals are very close to each other. The mean value for current harmonic integral is 100.22 and the standard deviation is 1.07. This means that the difference between synchronizing methods is of no importance when this control method is used.

The connection point voltages, converter currents and zoomed converter currents when SRF-PLL is used are shown in Figs. 8a, 8b and 8c, respectively. Same measures when DSOGI-FLL is used are shown in Figs. 8d, 8e and 8f. It can be seen that the converter currents in this case contain great amount of distortion and the performance is not dependent on the used synchronizing method.

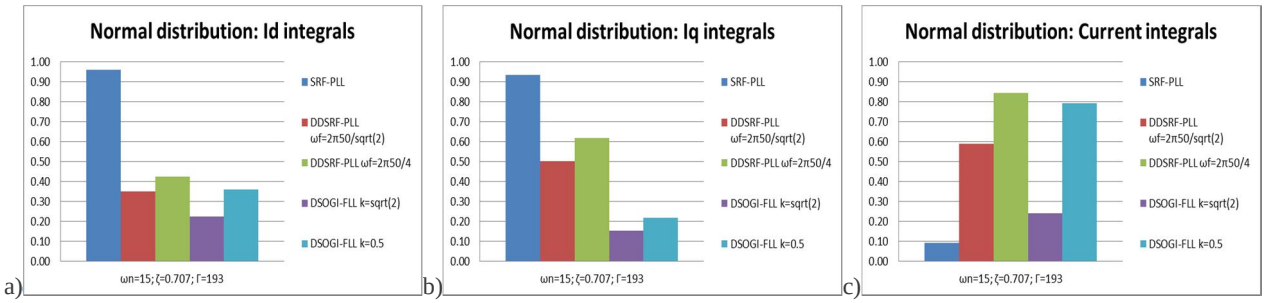

Fig. 7. a) d-axis current controller error integrals, b) q-axis current controller error integrals, c) harmonic integrals during phase to ground fault.

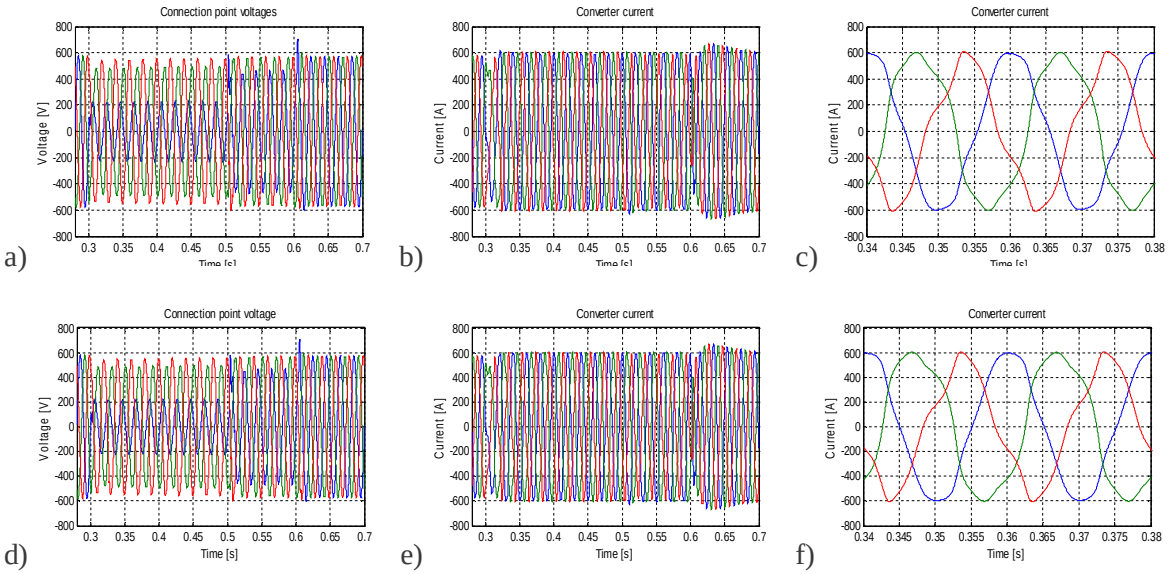

Fig. 8. SRF-PLL: a) connection point voltages, b) converter currents, c) zoomed converter currents; DSOGI-FLL: d) connection point voltages, e) converter currents, f) zoomed converter currents.

The converter current d-axis component and its reference are shown in Figs. 9a and 9c when SRF-PLL and DSOGI-FLL is used, respectively. The current reference is not although the i_{WT} is zero due to the operation of DC-link voltage controller. The q-axis components are shown in Figs. 9b and 9d. The difference between Figs. 5a and 5c as well as 5b and 5b are of no importance. However, independent of the method the difference between the reference and the measured value is remarkable. In other words, the current q- and especially d-axis component is not precisely controllable.

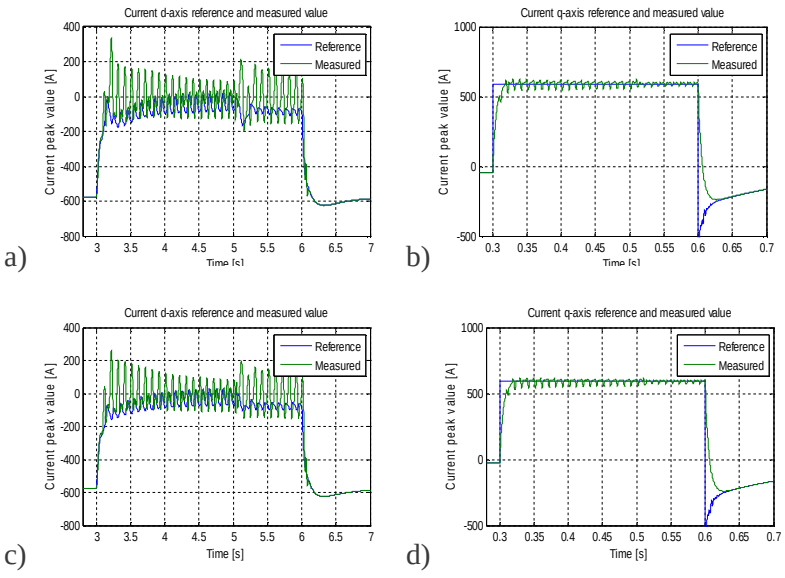

Fig. 9. SRF-PLL: a) d-axis converter current and its reference, b) q-axis converter current and its reference; DSOGI-FLL: c) d-axis converter current and its reference, d) q-axis converter current and its reference.

The frequency of the SRF-PLL during the grid fault is shown in Fig. 10a. Also here, the negative sequence component causes the 100 Hz oscillations. Thus, the converter current harmonics are generated by the DC-link voltage controller through variable d-axis current reference and variable frequency of the SRF-PLL

loop. The Fig. 10c shows that the angular frequency is nearly constant when DSOGI-FLL is used. However, due to the oscillating d-axis reference and current loop which amplifies the oscillations the converter current contains harmonics. The DC-link voltage and its reference values are shown in Figs. 10b and 10d when SRF-PLL and DSOGI-FLL is used, respectively. The difference between the results in 10b and 10d are of no importance.

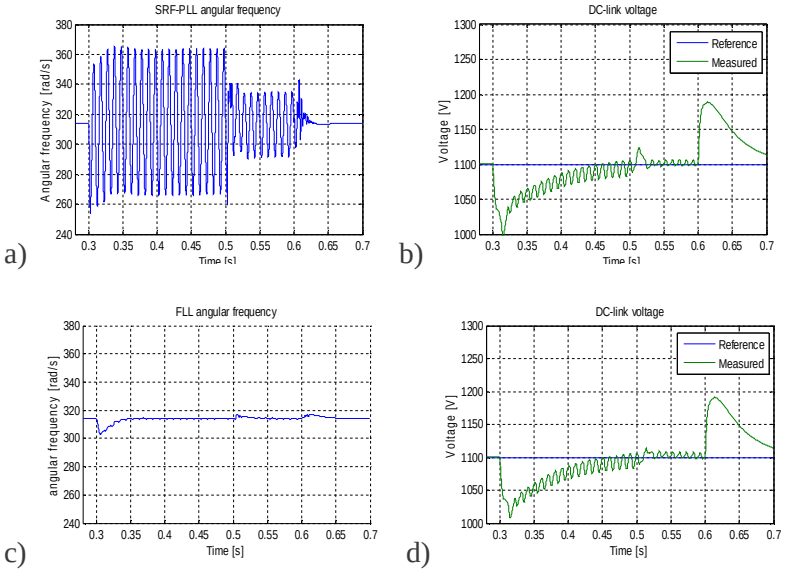

Fig. 10. SRF-PLL: a) angular frequency, b) DC-link voltage reference and measured value; DSOGI-FLL: c) angular frequency, d) DC-link voltage reference and measured value.

In order to explain the high amount of harmonics of wind turbine currents during one phase-to-ground fault using this control strategy the phasor diagram where relationships of U_{conv}, U_{sync} and I_{L1} are illustrated are shown in Fig. 11. In Fig. 11, L corresponds to the sum of inductances L_1 and L_2. The impact of LCL-filter capacitor to is neglected in order to simplify the figure. It can be seen that when i_q^* is controlled to zero the amplitude for U_{conv} needed to generate a certain current is much smaller than when the i_q^* is selected to be nominal. In other words, the amplitude of U_{conv} is smaller when active power is prioritized compared to reactive power prioritization. Due to the fact that the length of the voltage vector $\underline{u}_{sync}$ does not decrease dramatically as a result of the one-phase fault the length of the voltage vector $\underline{u}_{conv}$ should be relatively high when reactive power prioritization is used during the fault. However, the DC-link voltage sets a limit to the length of the $\underline{u}_{conv}$. In this study, it is assumed that the converter is operating in linear space vector modulation area so the maximum length of $\underline{u}_{conv}$ is: $|\underline{u}_{conv}|=u_{DC}/\mathrm{sqrt}(3)$. In the simulations, the $\underline{u}_{conv}$ saturates to the maximum available value during the fault. Thus, the currents cannot be controlled anymore which explains the converter current distortion independent on the used synchronizing method. [2][3]

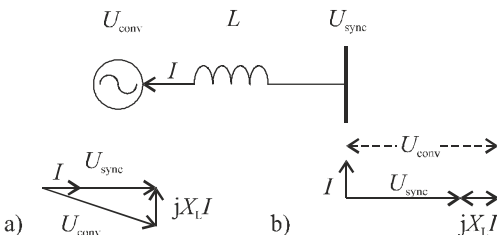

Fig. 11. Phasor diagram of current control: a) $i_q^* = 0$, b) $i_q^* =$ nominal.

Nominal active current with zero *q**

During the fault, the wind turbine is generating nominal active power while the aim of the reactive power control is to keep the connection point reactive power as a zero. The d- and q- axis current controller error integrals and harmonic integrals are shown in Fig. 12a, 12b and 12c. The best performance regarding to the harmonic integrals is achieved using DSOGI-FLL with SOGI gain *k*=0.5. The worst performance appears using SRF-PLL. The results in Fig. 12a are misleading due to the fact that the mean value for current d-axis error is 0.715 and the standard deviation is 0.075. This means that the difference between synchronizing methods is of no importance. The mean value for q-axis current error is 6.23 and the standard deviation is 0.5. Thus, the results in Fig. 12b are more illustrative. The mean value for current integrals shown in Fig. 12c is 28.87 and the standard deviation is 1.58.

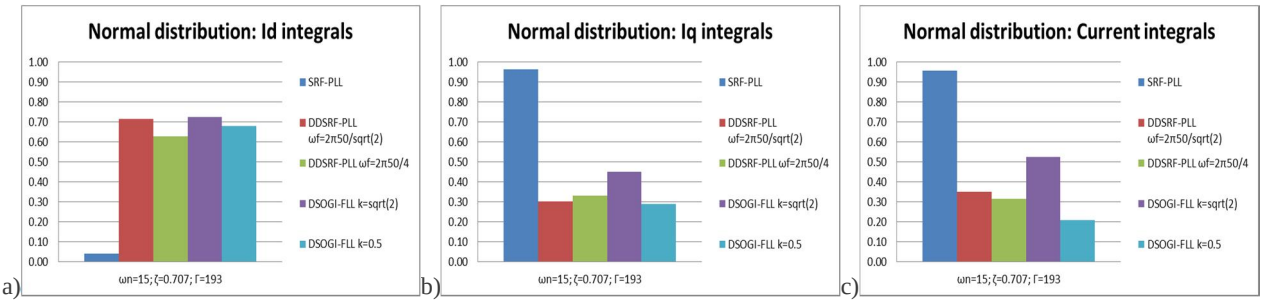

Fig. 12. a) d-axis current controller error integrals, b) q-axis current controller error integrals, c) harmonic integrals during phase to ground fault.

The connection point voltages, converter currents and zoomed converter currents when SRF-PLL is used are shown in Figs. 13a, 13b and 13c, respectively. Same measures when DSOGI-FLL is used are shown in Figs. 13d, 13e and 13f. It can be seen that the converter currents in this case contain great amount of distortion and the performance depends slightly on the used synchronizing method.

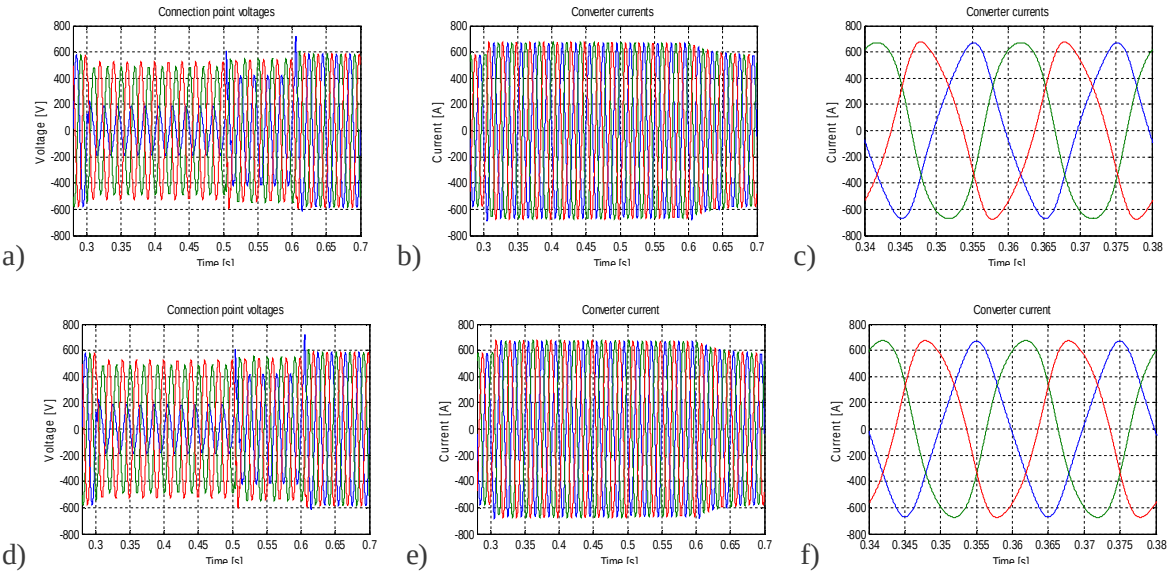

Fig. 13. SRF-PLL: a) connection point voltages, b) converter currents, c) zoomed converter currents; DSOGI-FLL: d) connection point voltages, e) converter currents, f) zoomed converter currents.

The converter current d-axis component and its reference are shown in Figs. 14a and 14c when SRF-PLL and DSOGI-FLL is used, respectively. The q-axis components are shown in Figs. 14b and 14d. The difference between Figs. 14a and 14c are of no importance. However, the current control in q-axis is improved greatly when the DSOGI-FLL is used. The harmonics in converter current appears as a result of the action of reactive power controller which causes non-constant i_q^*.

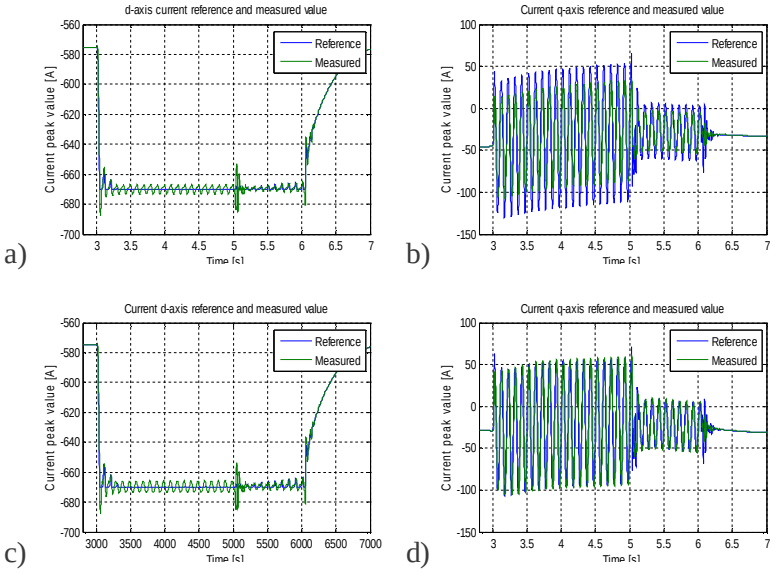

Fig. 14. SRF-PLL: a) d-axis converter current and its reference, b) q-axis converter current and its reference; DSOGI-FLL: c) d-axis converter current and its reference, d) q-axis converter current and its reference.

The frequency of the SRF-PLL during the grid fault is shown in Fig. 15a. Also here, the negative sequence component causes the 100 Hz oscillations. The Fig. 15c shows that the angular frequency is nearly constant when DSOGI-FLL is used. The DC-link voltage and its reference values are shown in Figs. 15b and 15d when SRF-PLL and DSOGI-FLL is used, respectively. The differences between the results are insignificant.

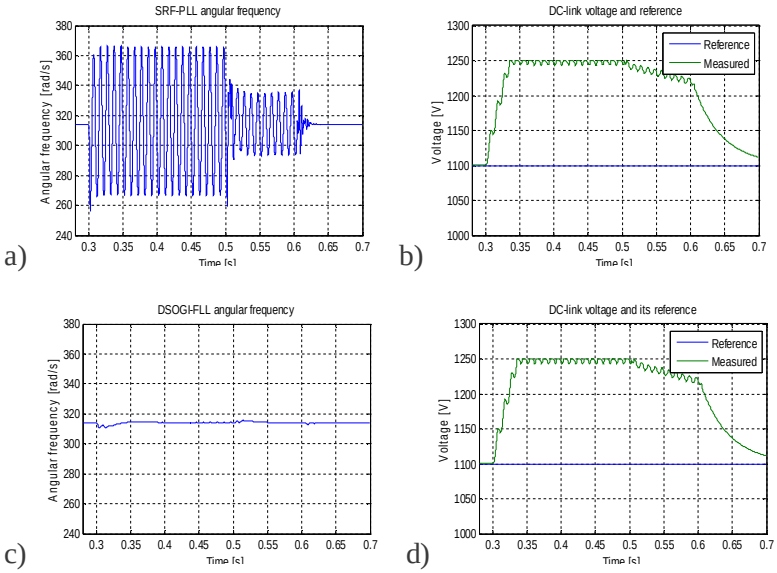

Fig. 15. SRF-PLL: a) angular frequency, b) DC-link voltage reference and measured value; DSOGI-FLL: c) angular frequency, d) DC-link voltage reference and measured value.

Conclusion

In this study, three different control methods of wind turbine during one phase to ground fault are compared. In addition, the impact of the used control methods, namely SRF-PLL, DDSRF-PLL and DSOGI-FLL, is evaluated. The used control methods during the fault are active power and reactive power prioritization as well as active power prioritization with reactive power control with aim of controlling the reactive power in connection point to zero.

When active power prioritization is used the active current reference i_d^* increases to its limiting value while the i_q^* is set to zero. The simulation results show that the wind turbine generates much more sinusoidal currents to the network during the fault when DSOGI-FLL or DDSRF-PLL is used. This happens because the synchronizing methods filter the effect of negative sequence component from the network voltage on the synchronizing angle.

When the reactive current reference i_q^* is set to nominal value during the fault the converter saturates due to the requirement of higher length of voltage vector $\underline{u}_{conv}$ that can be generated from the DC-link voltage. Thus, the currents fed to the network contain harmonics independent of the used synchronizing method.

When the active power is prioritized and the reactive power reference for reactive power controller is set to zero the DSOGI-FLL and DDSRF-PLL show better performance than SRF-PLL because of more linear operation of synchronizing angle. However, the negative sequence component of the network voltage interfere the converter operation through reactive power controller causing harmonics to the generated current by the wind turbine.

References

[1] A. S. Mäkinen, “Impact of synchronizing method on wind turbine operation”, SGEM deliverable D5.1.25, 2012, p. 55.

[2] N. Mohan, T. Undeland, W. Robbins, “Power electronics, converters, applications and desing”, John Wiley & Sons. INC, New Jersey, United States, 2003, p.802.

[3] D. P. Kothari, I. J. Nagrath, “Modern power system analysis” Third Edition, Tata McGraw-Hill Publishing Company Limited, New Delhi, 2003, p. 694.